Journal of Power Sources 196 (2011) 1127–1131

Contents lists available at ScienceDirect

Journal of Power Sources

journal homepage: www.elsevier.com/locate/jpowsour

Short communication

Carbon supported Pt–Y electrocatalysts for the oxygen reduction reaction

Min Ku Jeon, Paul J. McGinn*

Department of Chemical and Biomolecular Engineering, University of Notre Dame, Notre Dame, IN 46556, USA

ARTICLE INFO

Article history:
Received 27 June 2010
Received in revised form 17 August 2010
Accepted 17 August 2010
Available online 26 August 2010

Keywords:
Oxygen reduction reaction
Electrocatalyst
Polymer electrolyte membrane fuel cell
Rotating disk electrode

ABSTRACT

Carbon supported Pt_3Y (Pt_3Y/C) and PtY (PtY/C) were investigated as oxygen reduction reaction (ORR) catalysts. After synthesis via reduction by $NaBH_4$, the alloy catalysts exhibited 10–20% higher mass activity (mA mg_{Pt}^{-1}) than comparably synthesized Pt/C catalyst. The specific activity ($\mu A\ cm_{Pt}^{-2}$) was 23 and 65% higher for the Pt_3Y/C and PtY/C catalysts, respectively, compared to Pt/C. After annealing at 900 °C under a reducing atmosphere, Pt_3Y/C-900 and PtY/C-900 catalysts showed improved ORR activity; the Pt/C and Pt/C-900 (Pt/C catalyst annealed at 900 °C) catalysts exhibited specific activities of 334 and 393 $\mu A\ cm_{Pt}^{-2}$, respectively, while those of the Pt_3Y/C-900 and PtY/C-900 catalysts were 492 and 1050 $\mu A\ cm_{Pt}^{-2}$, respectively. X-ray diffraction results revealed that both the Pt_3Y/C and PtY/C catalysts have a fcc Pt structure with slight Y doping. After annealing, XRD showed that more Y was incorporated into the Pt structure in the Pt_3Y/C-900 catalyst, while the PtY/C-900 catalyst remained unchanged. Although these results suggested that the high ORR activity of the PtY/C-900 catalyst did not originate from Pt–Y alloy formation, it is clear that the Pt–Y system is a promising ORR catalyst which merits further investigation.

1. Introduction

Polymer electrolyte membrane fuel cells (PEMFCs) are under intensive research due to their promising application in fuel cell vehicles which utilize hydrogen and oxygen to produce electricity and water [1]. Although carbon supported Pt catalysts (Pt/C) exhibit high activity for hydrogen oxidation reaction, they suffer from relatively low activity for the oxygen reduction reaction (ORR). In addition, the high cost of Pt is a significant hurdle in commercialization of PEMFCs, such that it was suggested that the ORR activity per noble metal should be improved by a factor of 4 [2]. To achieve this goal, extensive efforts have been devoted to the development of cheap and highly active ORR electrocatalysts. A notable overview of the development of ORR electrocatalysts was authored by Gasteiger and Markovic [3]. Transition metal alloyed Pt catalysts including PtCo [4–12], PtNi [7,9,10,11,13], and PtFe [4,9,10,14,15] have been intensively investigated to improve upon the performance of Pt/C electrocatalysts. Further improvements have been realized through the use of de-alloyed PtCo [16,17] and PtCu [18] catalysts, Pt-free Fe–C–N catalyst [19], and Pt_3Ni (1 1 1) surfaces [13]. Although the binary Pt–M (M = early transition metals) alloys exhibit promising ORR activities, dissolution of M in the PEMFC environment [20–22] suggests that it is still worth searching for more active and stable alloys.

Recently, Greely et al. [23] employed a computational method to calculate the ORR activity of Pt_3M (M = transition metals) electrocatalysts. A Pt_3Y catalyst was reported as a promising ORR electrocatalyst, which was also verified by their bulk polycrystalline study. However, a carbon supported powder version of a Pt–Y electrocatalyst has not yet been reported. Hence, in the present study, carbon supported Pt_3Y and PtY catalysts were synthesized and characterized for the ORR.

2. Experimental

2.1. Synthesis of Pt–Y electrocatalysts

Initially, a conventional $NaBH_4$ reduction method was employed to synthesize Pt–Y electrocatalysts. $H_2PtCl_6{\cdot}6H_2O$ and $Y(NO_3)_3{\cdot}6H_2O$ were used as the Pt and Y precursors, respectively. The precursors were dissolved in a methanol and de-ionized (DI) water mixture (1:80, v/v), and then an appropriate amount of carbon support (Vulcan XC72R) was dispersed in the solution. The amount of carbon support was adjusted to get 20 wt.% metal loading (Pt + Y). The mixture was stirred for 30 min and then 0.2 M of $NaBH_4$ solution was added to the mixture as a reducer. The resulting mixture was further stirred for 1 h to confirm termination of reduction reaction followed by filtering. The resulting powder was washed with DI water and then dried in an oven at 100 °C overnight. The resulting electrocatalysts were denoted as Pt_3Y/C and PtY/C according to their ratio of precursors. To obtain more highly alloyed electrocatalysts, the Pt_3Y/C and PtY/C catalysts were annealed at 900 °C for 5 min under H_2/Ar flow (5.2 mol.% H_2). The

* Corresponding author. Tel.: +1 574 631 6151; fax: +1 574 631 8366.
E-mail address: mcginn.1@nd.edu (P.J. McGinn).

0378-7753/$ – see front matter © 2010 Elsevier B.V. All rights reserved.
doi:10.1016/j.jpowsour.2010.08.048

Table 1
Summary of XRD results. Results of Pt/C [27] and Pt/C-900 [24] catalysts were reported previously.

	(1 1 1) peak position (°)	*d* (nm)	Lattice parameter (nm)	Crystallite size (nm)
Pt/C [27]	39.41	0.2285	0.3958	2.4
Pt/C-900 [24]	39.70	0.2268	0.3928	3.3
Pt_3Y/C	39.82	0.2262	0.3918	5.4
Pt_3Y/C	40.21	0.2241	0.3882	33.2
PtY/C	39.84	0.2261	0.3916	4.7
PtY/C-900	39.72	0.2268	0.3928	17.0

resulting electrocatalysts are termed as Pt_3Y/C-900 and PtY/C-900 catalysts. Pt/C and Pt/C-900 catalysts were also synthesized via the same route for comparison [24].

2.2. Physical and electrochemical characterization

Structural analysis of the catalysts was performed by X-ray diffraction (XRD) between 20° and 80° 2-theta in a step scan mode (0.2° step). Scanning time was 0.5 s for each step.

A rotating disk electrode (RDE) technique [25] was employed for electrochemical analysis of the catalysts. A catalyst layer was formed on a glassy carbon electrode (0.159 cm^2 area) by dripping 20 μL of catalyst ink. The catalyst ink was prepared by mixing the catalyst, DI water, isopropyl alcohol, and Nafion ionomer solution. The ink was sonicated before deposition to achieve homogeneous mixing. After drying in air, dilute Nafion ionomer solution was dripped on the catalyst layer to provide mechanical strength. Loading of the catalyst was 209 $\mu g_{catal.}\ cm^{-2}$ for all the catalysts, which means Pt loading was 41.8, 36.3, and 28.7 $\mu g_{Pt.}\ cm^{-2}$ for the Pt/C, Pt_3Y/C, and PtY/C catalysts, respectively. Estimated thickness of the Nafion film was about 0.22 μm based on a Nafion density of 1.98 g cm^{-3} [26]. Electrochemical characterization was performed for cyclic voltammetry (CV) and ORR activity. The CV testing was performed by potential cycling between 0 and 1.2 V (vs. reversible hydrogen electrode (RHE)) for 50 cycles at a scan rate of 50 mV s^{-1}. Nitrogen purged 0.5 M H_2SO_4 solution was used as an electrolyte. Pt mesh and a saturated calomel electrode were used as the counter and reference electrodes, respectively. ORR activity was measured by potential sweep from 0.2 to 1.0 V (vs. RHE) at a sweep rate of 20 mV s^{-1}. Oxygen saturated 0.5 M H_2SO_4 solution was used as an electrolyte. For kinetic study of the catalysts, the ORR activity was measured at various rotation speeds of 400, 900, 1600, and 2500 rpm. All potentials in this paper were converted to RHE scale.

3. Results and discussion

The XRD results are shown in Fig. 1a along with the pertinent reference peaks in Fig. 1b. In the un-annealed Pt_3Y/C and PtY/C catalysts, only fcc Pt peaks were observed. Positions of the (1 1 1) peak were slightly shifted from 39.41° in the Pt/C catalyst [27] to 39.82° and 39.84° in the Pt_3Y/C and PtY/C catalysts, respectively, indicating that Y was slightly alloyed with Pt. After annealing at 900 °C, the peak shift was more significant. In the Pt_3Y/C-900 catalyst, the (1 1 1) peak was observed at 40.21°, which means more Y was incorporated into the fcc Pt structure. We could not observe any signs of secondary phases or phase transitions. On the other hand, Greely et al. [23] observed a lattice parameter of 0.4072 nm in their bulk polycrystalline sample, which is very close to the 0.4075 nm reference value for Pt_3Y (ICDD #00-017-0058). But, in the present study, the lattice parameter obtained from the Pt_3Y/C-900 catalyst was 0.3882 nm as listed in Table 1. In the PtY/C-900 catalyst, the (1 1 1) peak position moved in an opposite direction, and the peak was observed at 39.72°, which is very close to the 39.70° value for the

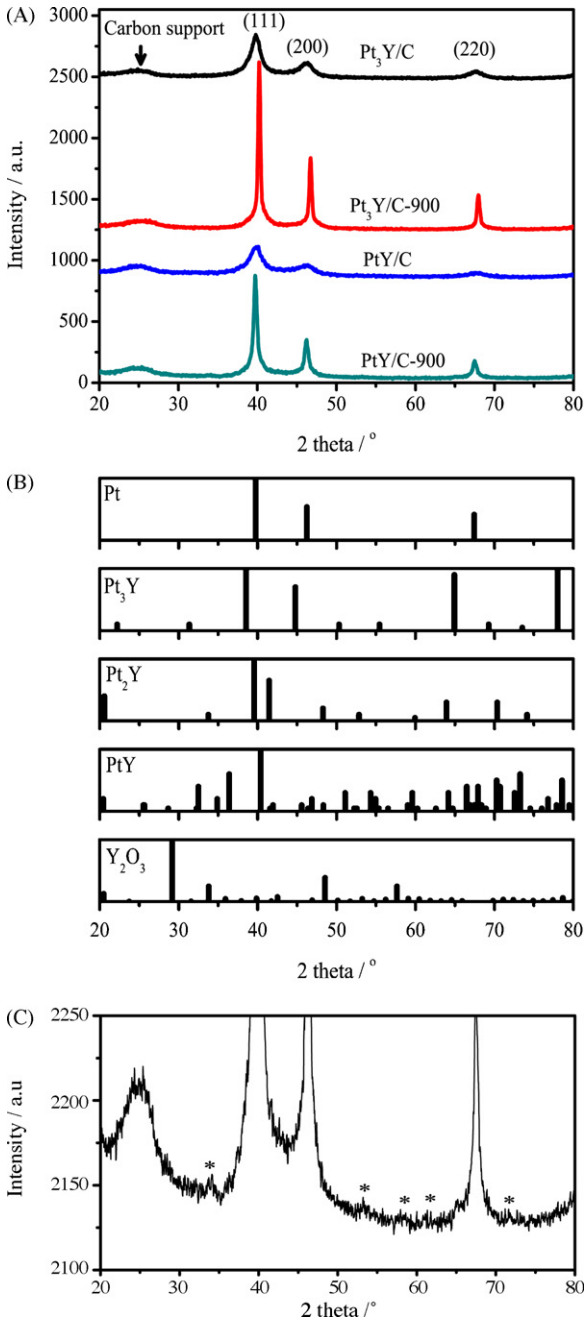

Fig. 1. (a) The XRD results of the Pt_3Y/C, Pt_3Y/C-900, PtY/C, and PtY/C-900 catalysts. (b) The XRD peak positions and intensities of pertinent reference phases including Pt (ICDD #03-065-2868), Pt_3Y (ICDD #00-017-0058), Pt_2Y (ICDD #00-012-0333), PtY (ICDD #00-019-0919), and Y_2O_3 (ICDD #01-071-0049). (c) Enlarged image of the XRD result of the PtY/C-900 catalyst.

Pt/C-900 catalyst. This result suggests that Y was not alloyed with Pt during the annealing in spite of the higher Y content than the Pt_3Y/C-900 catalyst. In addition, we could observe new peaks with small intensities as shown in Fig. 1c (denoted by asterisks). None of the Pt–Y alloys or Y_2O_3 peaks in the ICDD database matched with the peaks of the unknown phase(s). These results show that formation of the Pt_3Y phase is not as straightforward as other systems we have examined where we observed formation of, for example, PtCr [28] and Pt_3Ti [27] phases via same or similar annealing processes. Therefore, more investigation on the phase transition is desirable to clarify phase formation of Pt–Y alloys on carbon supports. The crystallite size of the catalysts was calculated using the

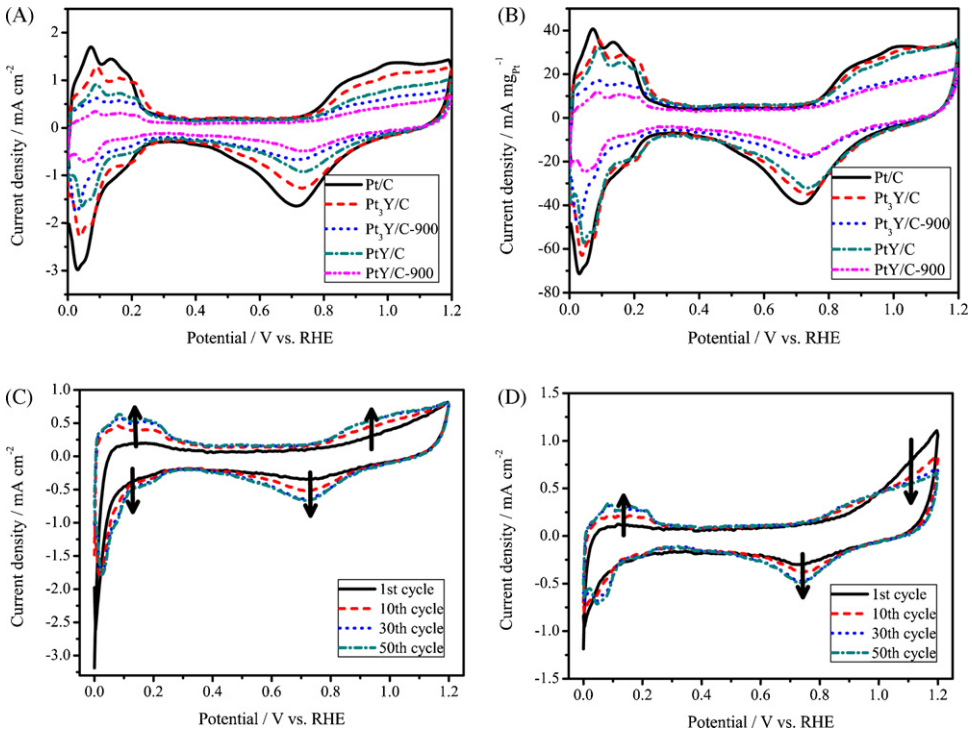

Fig. 2. (a) The CV results of the Pt_3Y/C, Pt_3Y/C-900, PtY/C, and PtY/C-900 catalysts. Previously reported result of the Pt/C catalyst was also included for comparison [24]. (b) Re-drawing of (a) based on Pt mass scale. The CV results according to number of cycles are shown for the (c) Pt_3Y/C-900 and (d) PtY-/C-900 catalysts. Testing was performed in nitrogen purged 0.5 M H_2SO_4 solution by potential cycling between 0 and 1.2 V for 50 cycles at a scan rate of 50 mV s^{-1}.

Scherrer equation, which resulted in 5.4, 33.2, 4.7, and 17.0 nm values for the Pt_3Y/C, Pt_3Y/C-900, PtY/C, and PtY/C-900 catalysts, respectively. Interestingly, the crystallite size of the Pt_3Y/C-900 catalyst was almost twice that of the PtY/C-900 catalyst meaning that composition is also an important parameter in the particle agglomeration. Detailed information from the XRD measurements is listed in Table 1.

The cyclic voltammetry results are shown in Fig. 2a. The result of the Pt/C catalyst which was reported previously [24] is also included for comparison. For a better comparison, Fig. 2a was also drawn in Pt mass scale as Fig. 2b. Significant changes were observed in the regions of hydrogen adsorption/desorption (0–0.3 V) and platinum oxidation/reduction (0.6–1.2 V). The alloy catalysts showed smaller area in these regions due to the decreased amount of surface Pt. Except for the Pt_3Y/C-900 catalyst, the other binary catalysts showed Pt-like behavior, presumably due to a low degree of Y alloying as discussed in the XRD results. During measurement of the CV data for 50 cycles, significant changes were observed in the 900 °C annealed catalysts. The changes are shown in Fig. 2c for the Pt_3Y/C-900 catalyst. In the first cycle of CV, the hydrogen desorption peak (0–0.3 V along the positive direction) was negligible, but it rapidly increased with an increasing number of cycles. In addition, a sharp peak was observed below 0.3 V along the negative scan direction, which is in agreement with the previous report [23]. The current density of this peak decreased after cycling which suggests that this peak is related to Y, and dissolution of surface Y occurs which provides more surface Pt. In the PtY/C-900 catalyst, shown in Fig. 2d, the changes during the CV testing were different from that of the Pt_3Y/C-900 catalyst. At first, the strong hydrogen adsorption peak below 0.3 V was not high relative to the Pt_3Y/C-900 catalyst, and after 30 cycles, the peak disappeared. This result means that a relatively small amount of Y was alloyed as discussed in the XRD results, and that the surface Y was quickly dissolved during the first 30 cycles. One more significant difference between the Pt_3Y/C-900 and PtY/C-900 catalysts was observed in the high potential region (0.8–1.2 V) along the positive scan direction. In the Pt_3Y/C-900 catalyst, the current density increased along the whole region while the current density at 1.2 V was almost constant. On the other hand, the current density at 1.2 V rapidly decreased with increasing cycles in the PtY/C-900 catalyst. These results show that Y was synthesized in different forms in the Pt_3Y/C-900 and PtY/C-900 catalysts, and the dissolution of surface Y has occurred during the CV, presumably via different mechanisms. Electrochemically active surface area (EAS) was also calculated from the CV results. The calculation was performed by integrating hydrogen desorption area by assuming a 210 μC cm^{-2} charge for desorption of a monolayer of hydrogen [29]. Although this value originated from polycrystalline Pt, it is still useful for comparison purpose. The calculated EAS values were 516, 245, 412, and 151 cm^2 $mg_{Pt}{}^{-1}$ for the Pt_3Y/C, Pt_3Y/C-900, PtY/C, and PtY/C-900 catalysts, respectively. Compared with 563 cm^2 $mg_{Pt}{}^{-1}$ in the Pt/C catalyst [24], the Pt_3Y/C catalyst did not show much difference in the EAS. On the other hand, the PtY/C catalyst showed a significant decrease in the EAS value, which might be due to strong surface segregation of Y during the $NaBH_4$ reduction step. Interestingly, the EAS value of the Pt_3Y/C-900 catalyst (245 cm^2 $mg_{Pt}{}^{-1}$) was more than 60% larger than the 151 cm^2 $mg_{Pt}{}^{-1}$ value of the PtY/C-900 catalyst, although the crystallite size of the Pt_3Y/C-900 catalyst was almost twice that of the PtY/C-900 catalyst. This result shows that the two catalysts (Pt_3Y/C-900 and PtY/C-900) have quite different bulk and surface properties as expected from the XRD and CV testing results.

Fig. 3 shows the RDE measurement results at a rotating speed of 1600 rpm. As shown in the figure, un-annealed catalysts showed similar or better activity for the ORR than the Pt/C catalyst. On the other hand, the Pt_3Y/C-900 catalyst exhibited a significant decrease in the ORR activity, while the decrease was less in the PtY/C-900 catalyst. A detailed investigation on the reaction mechanism was performed by applying the Koutecky–Levich (K–L) equation [25]:

$$\frac{1}{j} = \frac{1}{j_k} + \frac{1}{j_d} + \frac{1}{j_f} \quad (1)$$

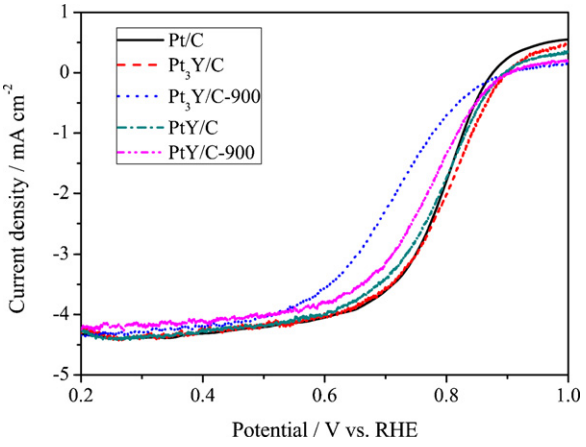

Fig. 3. The RDE testing results of the Pt_3Y/C, Pt_3Y/C-900, PtY/C, and PtY/C-900 catalysts recorded at a rotation speed of 1600 rpm. Testing was performed in oxygen saturated 0.5 M H_2SO_4 solution by potential sweep from 0.2 to 1.0 V at a scan rate of 20 mV s^{-1}.

where j_k is the kinetic controlled current density, j_d is the diffusion limited current density, and j_f is the Nafion film diffusion limited current density [30]. Here, the j_f term can be expressed as

$$j_f = \frac{nFc_fD_f}{L} \quad (2)$$

where n is the number of exchanged electrons in the reaction, F is Faraday's constant, c_f is the reactant concentration in the Nafion film, D_f is the diffusion constant in the Nafion film, and L is the Nafion film thickness. As noted above, L was about 0.22 μm, which is slightly thicker than the critical thickness of 0.20 μm where Nafion diffusion is not a rate-determining step [31]. But, 0.22 μm is still thin enough to have the $1/j_f$ term eliminated from Eq. (1) [24]. The j_d term can be expressed as

$$j_d = 0.62nFD^{2/3}\omega^{1/2}n^{-1/6}C_{O_2} \quad (3)$$

where D is the diffusion coefficient of O_2 (1.8×10^{-5} cm^2 s^{-1}), ω is the RDE rotation speed, ν is the kinematic viscosity (0.010 cm^2 s^{-1}), and C_{O_2} is the concentration of molecular oxygen (1.13×10^{-6} mol cm^{-3}) [32]. Eq. (3) can be simplified as

$$j_d = BC_{O_2}\omega^{1/2} \quad (4)$$

where $B = 0.62nFD^{2/3}\nu^{-1/6}$. Therefore, we employed following Eq. (5) for calculation of n and j_k values.

$$\frac{1}{j} = \frac{1}{j_k} + \frac{1}{BC_{O_2}\omega^{1/2}} \quad (5)$$

Linear fitting of Eq. (5) was performed using $1/j$ and $1/\omega^{1/2}$ as parameters so that n and j_k values could be derived from slope and intercept, respectively. The fitting results are shown in Fig. 4 with the RDE measurement results as a function of rotation speed shown as insets. The calculated values are listed in Table 2. For all samples, n values were 3.66–3.91 suggesting that a 4-electron reaction ($O_2 + 4e^- + 4H^+ \rightarrow 2H_2O$) is dominant in the binary catalysts. In the un-annealed catalysts, mass activities (mA mg_{Pt}^{-1}) were 10–20% higher than the Pt/C catalyst. In terms of specific activity (μA cm_{Pt}^{-2}), the Pt_3Y/C and PtY/C catalysts exhibited 23 and 65% higher activity than the Pt/C catalyst in spite of poor alloying between Pt and Y. In the annealed catalysts, a decrease in the mass activities was observed due to reduced EAS values. But when compared with the Pt/C-900 catalyst, the PtY/C-900 catalyst showed 27% higher mass activity. The PtY/C-900 catalyst exhibited high specific activity of 1050 μA cm_{Pt}^{-2}, which is more than 2.5 times higher than the Pt/C-900 (393 μA cm_{Pt}^{-2}) and Pt_3Y/C-900

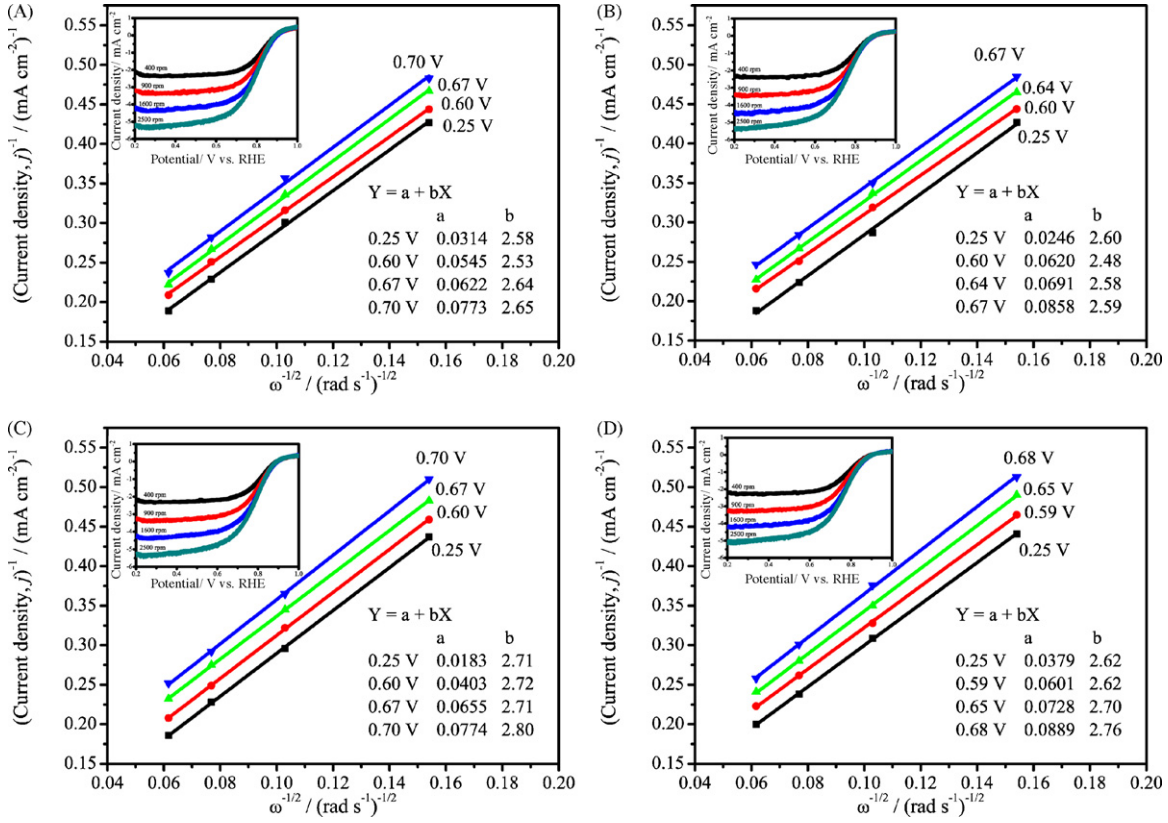

Fig. 4. The fitting results of Koutecky–Levich equation for the (a) Pt_3Y/C, (b) Pt_3Y/C-900, (c) PtY/C, and (d) PtY/C-900 catalysts. Insets illustrate the corresponding RDE measurement results which were performed for various rotation speeds of 400, 900, 1600, and 2500 rpm.

Table 2
Summary of electrochemical testing results. Current density values (j, j_k, $j_{k\text{-mass}}$, and $j_{k\text{-spec}}$) are calculated from 1600 rpm data at 0.75 V. The results of Pt/C and Pt/C-900 catalysts were reported previously [24].

	EAS ($cm^2\ mg_{Pt}^{-1}$)	j ($mA\ cm^{-2}$)	j_k ($mA\ cm^{-2}$)	$j_{k\text{-mass}}$ ($mA\ mg_{Pt}^{-1}$)	$j_{k\text{-spec}}$ ($\mu A\ cm_{Pt}^{-2}$)	n
Pt/C [24]	563	2.99	7.86	188	334	3.72
Pt/C-900 [24]	317	2.54	5.20	125	393	3.82
Pt_3Y/C	516	3.03	7.69	212	411	3.85
Pt_3Y/C-900	245	2.35	4.38	121	492	3.91
PtY/C	412	2.75	6.53	227	552	3.66
PtY/C-900	151	2.35	4.55	159	1050	3.75

($492\ \mu A\ cm_{Pt}^{-2}$) catalysts. In addition, the specific activity was a 3-fold improvement over the Pt/C catalyst ($334\ \mu A\ cm_{Pt}^{-2}$). Here, it should be recalled that the PtY/C-900 catalyst did not show any signs of alloying in the XRD results and exhibited Pt-like behavior in the CV results. Therefore, the improved ORR activity in the PtY/C-900 catalyst might have come from a different factor than the alloy formation of Pt–Y. Although the reason for the improved ORR activity in the PtY/C-900 catalyst is not yet clear, the high ORR activity of the Pt–Y catalysts suggests that they are promising ORR catalysts and worthy of further investigation.

4. Conclusion

Binary Pt_3Y/C and PtY/C catalysts were investigated for ORR activity. The XRD results revealed that Y was only slightly alloyed with Pt before annealing. After annealing, more Y was incorporated into the Pt structure in the Pt_3Y/C-900 catalyst, while no signs of alloying were observed in the PtY/C-900 catalyst. For the ORR, the catalysts showed slightly improved ORR activity both in mass ($mA\ mg_{Pt}^{-1}$) and specific ($\mu A\ cm_{Pt}^{-2}$) activity scales before the annealing. In the annealed catalysts, a significant increase in the ORR activity was observed in the specific activity scale. The specific activity of the PtY/C-900 catalyst ($1050\ \mu A\ cm_{Pt}^{-2}$) was more than 3.0 and 2.0 times higher than those of Pt/C ($334\ \mu A\ cm_{Pt}^{-2}$) and Pt_3Y/C-900 ($492\ \mu A\ cm_{Pt}^{-2}$) catalysts, respectively.

Acknowledgements

This work was partially supported by the U.S. Army CECOM RDEC through Agreement DAAB07-03-3-K414 and by the Department of Defense and the Army Research Office through contract numbers W911QX06C0117 and W911NF08C0037. Such support does not constitute endorsement by the U.S. Army of the views expressed in this publication.

References

[1] L. Carrette, K.A. Friedrich, U. Stimming, Fuel Cells 1 (2001) 5–39.
[2] H.A. Gasteriger, S.S. Kocha, B. Sompalli, F.T. Wagner, Appl. Catal. B: Environ. 56 (2005) 9–35.
[3] H.A. Gasteiger, N.M. Marković, Science 324 (2009) 48–49.
[4] Y. Qian, W. Wen, P.A. Adcock, Z. Jiang, N. Hakim, M.S. Saha, S. Mukerjee, J. Phys. Chem. C 112 (2008) 1146–1157.
[5] H.T. Duong, M.A. Rigsby, W.-P. Zhou, A. Wieckowski, J. Phys. Chem. C 111 (2007) 13460–13465.
[6] S. Koh, J. Leisch, M.F. Toney, P. Strasser, J. Phys. Chem. C 111 (2007) 3744–3752.
[7] U.A. Paulus, A. Wokaun, G.G. Scherer, T.J. Schmidt, V. Stamenkovic, V. Radmilovic, N.M. Markovic, P.N. Ross, J. Phys. Chem. B 106 (2002) 4181–4191.
[8] H. Yano, J.M. Song, H. Uchida, M. Watanabe, J. Phys. Chem. C 112 (2008) 8372–8380.
[9] H. Yano, M. Kataoka, H. Yamashita, H. Uchida, M. Watanabe, Langmuir 23 (2007) 6438–6445.
[10] L. Xiong, A. Manthiram, J. Electrochem. Soc. 152 (2005) A697–A703.
[11] S. Mukerjee, S. Srinivasan, J. Electroanal. Chem. 357 (1993) 201–224.
[12] S. Chen, W. Sheng, N. Yabuuchi, P.J. Ferreira, L.F. Allard, Y. Shao-Horn, J. Phys. Chem. C 113 (2009) 1109–1125.
[13] V.R. Stamenkovic, B. Fowler, B.S. Mun, G. Wang, P.N. Ross, C.A. Lucas, N.M. Markovic, Science 315 (2007) 493–497.
[14] M. Wakisaka, H. Suzuki, S. Mitsui, H. Uchida, M. Watanabe, J. Phys. Chem. C 112 (2008) 2750–2755.
[15] A.R. Malheiro, J. Perez, H.M. Villullas, J. Electrochem. Soc. 156 (2009) B51–B58.
[16] K.C. Neyerlin, R. Srivastava, C. Yu, P. Strasser, J. Power Sources 186 (2009) 261–267.
[17] R. Srivastava, P. Mani, N. Hahn, P. Strasser, Angew. Chem. Int. Ed. 46 (2007) 8988–8991.
[18] S. Koh, N. Hahn, C. Yu, P. Strasser, J. Electrochem. Soc. 155 (2008) B1281.
[19] M. Lefèvre, E. Proietti, F. Jaouen, J.-P. Dodelet, Science 324 (2009) 71–74.
[20] S. Chen, H.A. Gasteiger, K. Hayakawa, T. Tada, Y. Shao-Horn, J. Electrochem. Soc. 157 (2010) A82–A97.
[21] K.J.J. Mayrhofer, K. Hartl, V. Juhart, M. Arenz, J. Am. Chem. Soc. 131 (2009) 16348–16349.
[22] E. Antolini, J.R.C. Salgado, E.R. Gonzalez, J. Power Sources 160 (2006) 957–968.
[23] J. Greely, I.E.L. Stephens, A.S. Bondarenko, T.P. Johansson, H.A. Hansen, T.F. Jaramillo, J. Rossmeisl, I. Chorkendorff, J.K. Nørskov, Nat. Mater. 1 (2009) 552–556.
[24] M.K. Jeon, Y. Zhang, P.J. McGinn, Electrochim. Acta 55 (2010) 5318–5325.
[25] A.J. Bard, L.R. Faulkner, Electrochemical Methods: Fundamentals and Applications, second ed., John Wiley & Sons, New York, NY, 2001.
[26] H. Schulenburg, E. Müller, G. Khelashvili, T. Roser, H. Bönnemann, A. Wokaun, G.G. Scherer, J. Phys. Chem. C 113 (2009) 4069–4077.
[27] M.K. Jeon, P.J. McGinn, J. Power Sources 195 (2010) 2664–2668.
[28] M.K. Jeon, P.J. McGinn, J. Power Sources 194 (2009) 737–745.
[29] T. Biegler, D.A.J. Rand, R. Woods, J. Electroanal. Chem. 29 (1971) 269–277.
[30] D.R. Lawson, L.D. Whiteley, C.R. Martin, M.N. Szentimay, J.I. Song, J. Electrochem. Soc. 135 (1988) 2247–2253.
[31] M. Watanabe, H. Igarashi, K. Yosioka, Electrochim. Acta 40 (1995) 329–334.
[32] J. Jiang, B. Yi, J. Electroanal. Chem. 577 (2005) 107–115.